PAPER

Check for updates

Construction of a Au@MoS₂ composite nanosheet biosensor for the ultrasensitive detection of a neurotransmitter and understanding of its mechanism based on DFT calculations†

Kaida Lu,‡[a] Jiamei Liu,‡[a] Xinyue Dai, [b] Li Zhao,[a] Yufei Yang,[a] Hui Li [a] and Yanyan Jiang [*ac]

MoS₂ nanosheets can be applied as electrochemical biosensors to selectively and sensitively respond to the surrounding environment and detect various biomolecules due to their large specific surface area and unique physicochemical properties. In this paper, single-layer or few-layer MoS₂ nanosheets were prepared by an improved liquid phase stripping method, and then combining the unique material characteristics of MoS₂ and the metallic property of Au nanoparticles (AuNPs), Au@MoS₂ composite nanosheets were synthesized based on MoS₂ nanosheets. Then, the structure and properties of MoS₂ nanosheets and Au@MoS₂ composite nanosheets were comprehensively characterized. The results proved that AuNPs were successfully loaded on MoS₂ nanosheets. At the same time, on the basis of the successful preparation of Au@MoS₂ composite nanosheets, an electrochemical biosensor targeting dopamine was successfully constructed by cyclic voltammetry. The linear detection range was 0.5–350 μM, and the detection limit was 0.2 μM. The high-sensitive electrochemical detection of dopamine has been achieved, which provides a new idea for the application of MoS₂-based nanomaterials in the biosensing of neurotransmitters. In addition, density functional theory (DFT) was used to explore the electrochemical performance of Au@MoS₂ composite nanosheets. The results show that the adsorption of Au atoms on the MoS₂ 2D structure improves the conductivity of MoS₂ nanosheets, which theoretically supports the possibilities of its application as a platform for the ultrasensitive detection of neurotransmitters or other biomolecules in the field of disease diagnosis.

1. Introduction

Transition metal disulfides are other important two-dimensional materials besides graphene. Among them, MoS₂ as the most typical transition metal disulfide, has received extensive attention due to its ultra-thin structure and special physicochemical properties.[1–3] At present, single-layer or few-layer MoS₂ nanosheets, considered as semiconductor analogs of graphene, have been widely used in photochemistry, electrochemistry and long-acting transistor biosensors due to their high specific surface area, conductive photothermal conversion performance and easy functionalization.[4–7] Molybdenum

disulfide, combined with fluorescence, electrochemistry, surface-enhanced Raman spectroscopy and field-effect transistor technology, is considered to be a promising sensing platform for chemical/biological molecule detection.[5,7] Molybdenum disulfide nanosheets have been proven to be promising support materials for the modification of noble metal nanoparticles such as gold, silver, platinum, and palladium nanoparticles, and noble metal nanostructures are also considered ideal detection platforms for unlabeled and ultra-sensitive detection.[8,9] Wang et al. constructed a sandwich-type immunosensor for the detection of carcinoembryonic antigen (CEA) using the catalytic activity of MoS₂–Au nanocomposites, which could detect carcinoembryonic antigen as low as 0.27 pg ml⁻¹.[10] Su et al. successfully used AuNPs-MoS₂ as an electrochemical sensing platform for the detection of chemical/biological molecules including neurotransmitters, H₂O₂, ATP, thrombin, and protein.[11] Therefore, molybdenum disulfide based nanocomposites are potential biosensing nanomaterials.[12–14]

Neurotransmitter is a small molecule that transmits chemical information between brain cells through the process of nerve transmission, and its abnormal level is closely related to

[a] Liquid-Solid Structural Evolution & Processing of Materials (Ministry of Education), School of Materials Science and Engineering, Shandong University, Jinan, Shandong, 250061, P. R. China. E-mail: yanyan.jiang@sdu.edu.cn

[b] School of Life Sciences, Shanghai University, Shanghai, 200444, P. R. China

[c] Shenzhen Research Institute of Shandong University, Shenzhen, Guangdong, 518000, P. R. China

† Electronic supplementary information (ESI) available. See DOI: 10.1039/d1ra07962j

‡ The authors contributed equally to this work.

the occurrence of many mental disorders.[15] Dopamine is one of the most important neurotransmitters, whose reduction is directly related to nervous system diseases such as Parkinson's disease,[16,17] thus it is highly desirable to detect dopamine and other neurotransmitters accurately and rapidly in medical diagnosis.[18,19] Current detection of dopamine rely primarily on time-consuming and expensive liquid chromatography and molecular spectroscopy.[20] Compared with electrochemical methods,[21] electrochemical methods are significantly superior to other methods due to their simplicity, convenience, speed, and low cost.[22,23] Therefore, the research on the sensitive electrochemical method for the determination of dopamine is a hot topic at present. The efficient and rapid detection of dopamine has a positive effect on the survival and development of human beings.

Electrochemical detection is a convenient and rapid method, and many current detection methods are based on the physicochemical properties, biological properties and immunological properties.[24] Self-assembled nanoparticles modified electrode has attracted much attention because of its high sensitivity and stability.[25–27] As a typical two-dimensional material, MoS_2 has great potential for its application in the field of sensing.[28] Yang *et al.* demonstrated the application prospects of molybdenum disulfide hybrid materials in chemical/biomolecular sensing by culturing molybdenum disulfide flake-like nanostructures on polypyrrole microtubes.[29] Zheng *et al.* prepared a molybdenum disulfide modified carbon nanotube doped with nitrogen for the detection of hydrogen peroxide and ascorbic acid.[30] In the process of research, researchers realized that there were few active sites in single MoS_2 nanosheets, and the higher surface energy and the van der Waals interaction between layers caused serious aggregation of MoS_2. In order to improve the performance of the sensor, many researchers use surface modified electrodes for electrochemical detection.[31,32] Among them, the noble metal (such as Au and Ag) is loaded on the molybdenum disulfide nanosheets by the good synergy between the noble metal and the molybdenum disulfide nanosheets.[29] Rees *et al.* have developed a carbon nanopeptide electrode, which can detect dopamine in the range of 0.1 to 10 μM with a detection limit of 25 nM. Although their work proves that carbon-based nano-electrodes can be used for neurotransmitter detection, the sensitivity of the sensor needs to be further improved.[33] Alexander *et al.* developed an electrochemical sensor for dopamine detection by planting carbon nanotips on metal wires. Although the results reached the detection limit of 1 μM, the sensitivity was not ideal.[34] Tang *et al.* improved acupuncture needles with gold nanoparticles on the tip surface, and then electrochemically deposited graphene for dopamine detection. Due to the promotion of graphene and gold nanoparticles, the conductivity and sensitivity of the sensor were improved, but the detection limit was not minimized.[35] Choo *et al.* developed a 3D porous graphene oxide composite with gold nanoparticles for dopamine detection. The detection limit is 1.28 μM, and the linear response range is from 0.1 μM to 30 μM. However, this method has no significant signal changes in the detection of glucose and anti-bad blood glucose acid.[36] In this paper, in order to achieve the goals of low cost,

high sensitivity and more accurate detection limit, the electrochemical biosensor was constructed by modifying Au nanoparticles on MoS_2 nanosheets. The comparative experiments were performed using three kinds of electrodes, namely, a glassy carbon electrode (bare GCE), a MoS_2 nanosheet-modified glassy carbon electrode (MoS_2/GCE) and an Au@MoS_2 composite nanosheet-modified glassy carbon electrode (Au@MoS_2/GCE). The composite nanosheets has excellent conductivity and electrocatalytic performance due to the synergistic effect of the MoS_2 nanosheets and the Au nanoparticles,[37] thereby effectively promoting electron transfer between the redox probe and the electrode surface,[38] and achieves ideal detection performance.

In this work, we have constructed an electrochemical biosensor based on Au@MoS_2 composite nanosheets to achieve the specific and high-sensitivity quantitative electrochemical detection of dopamine, as shown in Scheme 1, which includes the preparation of MoS_2 nanosheets and Au@MoS_2 nanosheets as well as the detection of the model neurotransmitter molecules (dopamine). Transmission electron microscope (TEM), ultraviolet-visible spectrophotometer (UV-Vis), Fourier transform infrared spectrometer (FTIR), Raman Spectrometer (Raman), X-ray powder diffractometer (XRD) and X-ray photoelectron spectroscopy (XPS) were used to characterize the Au@MoS_2 composite nanosheets, and the results showed that the electrocatalytic performance of electrochemical detection was improved after AuNPs was successfully loaded on MoS_2 nanosheets, so that dopamine could be detected more effectively. The MoS_2-based biosensing platform can become a promising biomolecular detection method for biomedical applications.

2. Experimental section

2.1 Reagents and materials

Na_2HPO_4 and NaH_2PO_4 were purchased from Sinopharm Chemical Reagent Co., Ltd. Phosphate buffer (PBS, 0.1 M, pH 6.0–8.0) solution was prepared from stock solutions of Na_2HPO_4 and NaH_2PO_4. Dopamine (DA), gold (III) tetrachloride trihydrate ($HAuCl_4 \cdot 3H_2O$, 99%), sodium cholate, sodium citrate and molybdenum (IV) sulfide powder (<2 μm, 99%), were purchased from Sigma-Aldrich. Aqueous solutions were prepared with ultrapure water from Millipore system (>18 MΩ). All chemicals were directly used without further purification.

2.2 Apparatus and measurements

Ultrasonic treatment of molybdenum disulfide samples to obtain dispersed MoS_2 nanosheets was used an ultrasonic cell crusher (JY92-IIDN, Ningbo Xinzhi Biotechnology Co., Ltd., China). Morphologies of as-prepared products were performed with a HT-7700 transmission electron microscope (HT-7700, HITACHI, Japan). A UV-Vis spectrophotometer (SPECORD 200 PLUS, Jena, Germany) was used to determine the characteristic absorption peaks of the samples. A spectrometer (Nicolet 6700, Thermo Scientific) was used to obtain the data of Fourier transform infrared spectrometer (FTIR). The degree of
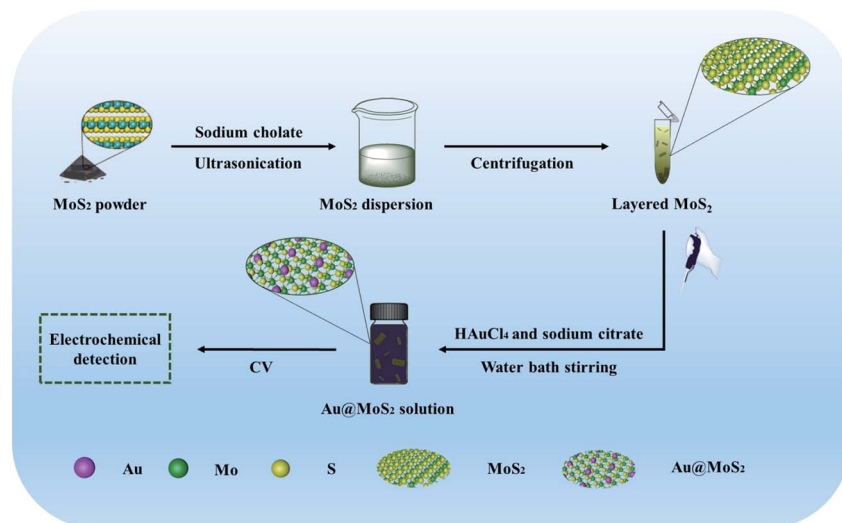
Scheme 1 The manufacturing process of MoS_2 nanosheets and $Au@MoS_2$ nanosheets and detection of the nanosheets.
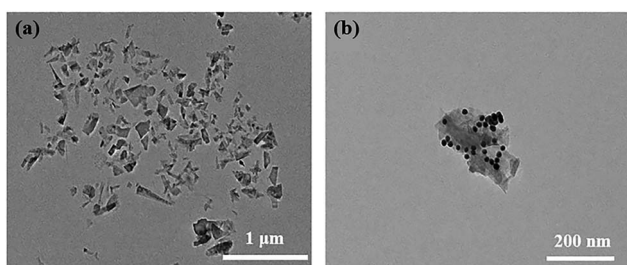

Fig. 1 TEM images of (a) dispersion of MoS_2 nanosheets and (b) $Au@MoS_2$ composite nanosheets.

exfoliation of the nanosheets was determined using a Raman spectrometer (Refence 3000+ iRaman, Gamry Instruments, USA). The X-ray diffraction (XRD) patterns of samples were verified by a X-ray electron diffractometer (D8 DISCOVER, Rigaku Corporation). X-ray photoelectron spectroscopy (XPS) was conducted by a spectrometer (ESCALAB 250Xi, Thermo Electron, USA) to investigate the surface elemental states of products. Electrochemical analysis of dopamine was performed on $Au@MoS_2$ composite nanosheets using an electrochemical workstation (DH7000, Jiangsu Donghua Analytical Instruments CO., Ltd., China).

2.3 Preparation of MoS_2

Layered MoS_2 was obtained through sonication-assisted exfoliation of bulk MoS_2 crystals in aqueous surfactant solution.[39–41] First, 250 mg of MoS_2 powder and 75 mg of sodium cholate were added into a 50 ml aqueous solution, and then the mixed solution was subjected to ultrasonic crushing (ultrasound effective time is 3 h under the condition of 50% power + ultrasound effective time is 2 h under the condition of 70% power) in an ice-water bath to obtain a black-green MoS_2 nanosheet dispersion. Subsequently, the resultant dispersion was centrifuged at 3000 rpm for 30 min, followed by the separation of the yellow-green supernatant to

remove the bulk MoS_2. The separated supernatant was centrifuged at 12 000 rpm (30 min) for the isolation of layered MoS_2. In order to remove sodium cholate adsorbed on the surface of nanosheet, the layered MoS_2 collected was dispersed in ultrapure water with the assistance of sonication. Similarly, the regenerated dispersion was centrifuged at 12 000 rpm for 30 min, followed by the collection of sediments to complete the washing process. The washing process was then repeated a further two times to remove sodium cholatecompletely. Ultimately, the sediments were dispersed in a certain amount of ultrapure water to prepare uniform layered MoS_2 dispersion. Furthermore, in order to obtain a high reproducibility for optical absorption detection, the stock solution of layered MoS_2 should be used after sonication treatment for 2 min.

2.4 Preparation of $Au@MoS_2$ nanocomposite decorated electrode

The method of preparing composite nanosheets by growing AuNPs on the prepared MoS_2 nanosheets is a typical self-assembly experiment.[16,42–44] First, 500 μL MoS_2 nanosheets dispersion of 1 mg ml^{-1} was added into a 10 ml glass bottle, and then 1 ml of 24.3 mmol $HAuCl_4$ solution was added into the bottle. The mixture was ultrasonicated for 5 min to form a uniform mixture. Then, 3 ml of sodium citrate solution with a concentration of 34 mmol was added to the above mixture, and the glass bottle was moved to a water bath under the condition of 96 °C with magnetic stirring until a uniformly dispersed black-purple mixed solution was obtained. The mixed solution was centrifuged at 10 000 rpm, and the precipitate was collected and cleaned repeatedly with deionized water several times to remove the excess impurities. Finally, the prepared $Au@MoS_2$ composite nanosheets were dispersed into deionized water for later use. The GCE of 3 mm in diameter was polished mechanically with 0.3 mm and 0.05 mm alumina powders and rinsed with ultrapure water between each polishing step. After this, it was sonicated with absolute ethanol and ultrapure water for about 1 min, respectively. 5 ml of the
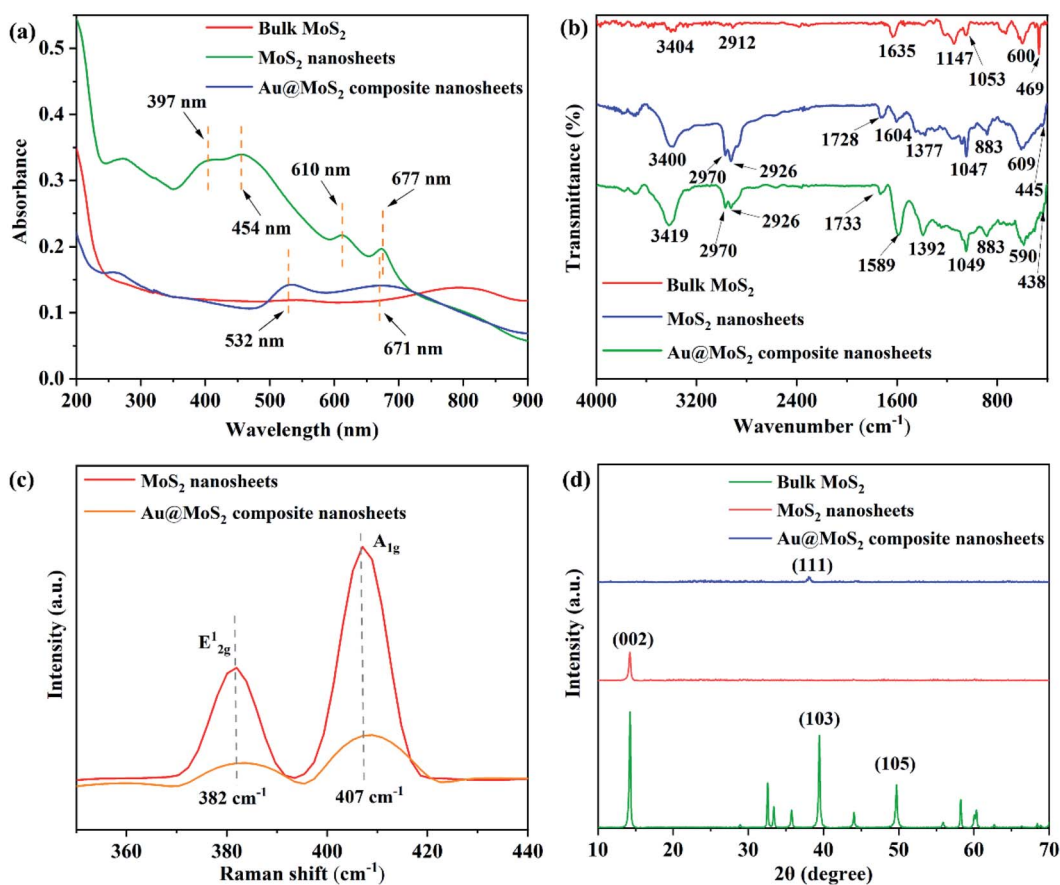
Fig. 2 (a) UV-vis absorption spectra of bulk MoS_2, MoS_2 nanosheets and $Au@MoS_2$ composite nanosheets; (b) FT-IR specta of bulk MoS_2, MoS_2 nanosheets and $Au@MoS_2$ composite nanosheets; (c) Raman spectra of MoS_2 nanosheets and $Au@MoS_2$ composite nanosheets; (d) XRD pattern of bulk MoS_2, MoS_2 nanosheets and $Au@MoS_2$ composite nanosheets.

$Au@MoS_2$ solution was dropped to the surface of the GCE and allowed to dry in the ambient air for about 16 h, which denotes as MoS_2/GCE. The electrodeposition method: pulse voltammetry (1.1–0.2 V), scan rate: 100 mV s^{-1}. For comparison, the AuNPs/GCE was prepared under the same condition.

2.5 Structural optimization of theoretical calculation

The density grid cutoff value of electrostatic potential is set to 65 Hartree, and the electron temperature in Fermi function is set to 300 K. To ensure the accuracy of calculation, double zeta plus polarization (DZP) basis set is adopted for all atoms involved. Set K point in Brillouin zone to $5 \times 5 \times 1$. In order to avoid the interaction between periodic structures, the model is built in a vacuum layer with more than 15 Å. Until the force acting on each atoms is less than 0.05 Å^{-1}, the structural optimization is completed.

3. Results and discussion

3.1 Characterization of MoS_2 nanosheets and $Au@MoS_2$ composite nanosheets

The morphologies of MoS_2 nanosheets and $Au@MoS_2$ composite nanosheets were characterized by transmission

electron microscopy. Fig. 1(a) confirms that the MoS_2 nanosheets have a wrinkled nanosheet structure, which indicates the formation of nanosheets of few layers or single layers with uniform size and good dispersibility, and the size of its planar sheet layers is about 150 nm. The as-prepared MoS_2 nanosheets have a large specific surface area and can provide a large one-sided space for the loading of AuNPs.

As shown in Fig. 1(b), many AuNPs with a uniform size and an average diameter of 20 nm are loaded on the MoS_2 nanosheets, suggesting $Au@MoS_2$ composite nanosheets had been successfully synthesized.[10,38,45] In addition, the growth of AuNPs on MoS_2 nanosheets does not damage the lamellar structure of MoS_2 nanosheets, but increases the specific surface area of the nanosheets, which provides good support for subsequent applications.

To further monitor the formation of $Au@MoS_2$ composite nanosheets, the UV-vis absorption spectra, FT-IR, Raman spectra and XRD of bulk MoS_2, MoS_2 nanosheets and $Au@MoS_2$ composite nanosheets were also investigated.

As shown in Fig. 2(a), there is no obvious characteristic optical absorption peaks appearing in the dispersion of bulk MoS_2 within the range of 200–800 nm, while a pair of obvious characteristic absorption peaks appear in the dispersion of
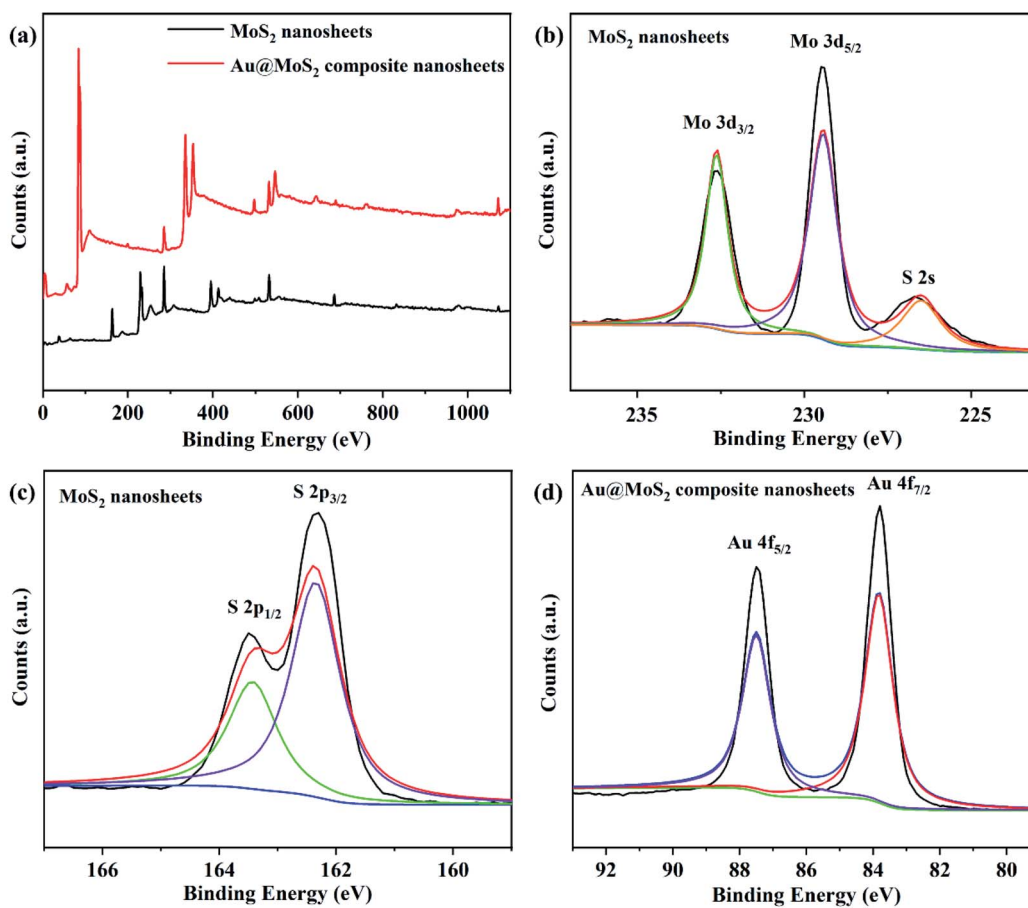
RSC Advances

Paper

Fig. 3 XPS spectra of MoS_2 nanosheets and Au@MoS_2 composite nanosheets. (a) Survey spectra of MoS_2 nanosheets and Au@MoS_2 composite nanosheets; (b) high resolution Mo 3d of MoS_2 nanosheets; (c) high resolution S 2p of MoS_2 nanosheets; (d) high resolution Au 4f of Au@MoS_2 composite nanosheets.
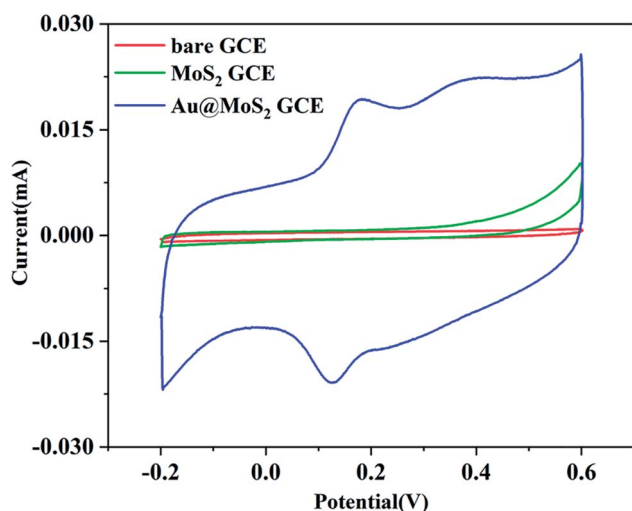

Fig. 4 CV curves of bare GCE, MoS_2/GCE and Au@MoS_2/GCE in PBS containing 150 µM DA.

MoS_2 nanosheets at 610 nm and 677 nm, which can be attributed to the A1 and B1 absorption bands of MoS_2, corresponding to two different transition modes of K points in the Brillouin zone in MoS_2 nanosheets. While the absorption peaks at 454 nm and 397 nm correspond to direct exciton transitions at M point between higher density in the band structure state region. The above results can preliminarily prove the success of the preparation of MoS_2 nanosheets.

Compared with MoS_2 nanosheets, the absorption peaks in the dispersion solution of Au@MoS_2 composite nanosheets disappear at 454 nm and 397 nm, while a new strong absorption peak corresponding to the surface plasmon resonance of AuNPs appears at 532 nm, which can prove the successful preparation of Au@MoS_2 composite nanosheets.

FT-IR spectrum has been also applied to monitor the formation of Au@MoS_2 composite nanosheets. As shown in Fig. 2(b), the bulk MoS_2 exhibits strong characteristic absorption peaks at the positions of 3404 cm^{-1} and 1635 cm^{-1} corresponding to hydroxyl groups, and another two strong absorption peaks at 469 cm^{-1} and 600 cm^{-1} correspond to the vibrations of the Mo–S bond.[46] Compared with bulk MoS_2, two positions of 2970 cm^{-1} and 2926 cm^{-1} correspond to the stretching vibration of C–H, and the positions of 1604 cm^{-1}, 1377 cm^{-1} and 1047 cm^{-1} correspond to the skeletal telescopic vibration of ΣC=C aromatic ring, the C–H symmetrical
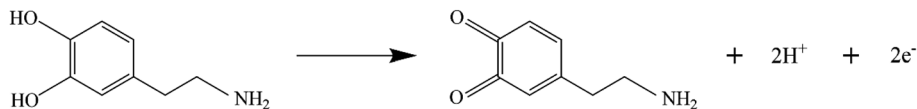
Fig. 5 The electrochemical reaction process of DA.

bending vibration of methyl group and the stretching vibration of C–O. The position of 883 cm^{-1} corresponds to the bending vibration of σC–H. All these can be attributed to the characteristic vibration of the functional group of the surfactant sodium cholate.

In addition, compared with the MoS$_2$ nanosheets, the absorption peak at the position of 1604 cm^{-1} representing the skeletal telescopic vibration of the σC=C aromatic ring disappeared. In addition, two strong new absorption peaks appear at 1589 cm^{-1} and 1392 cm^{-1} which correspond to the asymmetric telescopic vibration and the symmetric telescopic vibration of the C–O bond in the carboxylate, respectively. The above changes confirmed the formation of AuNPs on the surface of the MoS$_2$ nanosheets.

As shown in Fig. 2(c), Raman spectra of the MoS$_2$ nanosheets and Au@MoS$_2$ composite nanosheets were measured. The two Raman characteristic peaks corresponding to the two vibration modes of E$_{2g}^1$ and A$_{1g}$ are respectively located at 382 cm^{-1} and 407 cm^{-1}, and the displacement difference between the two characteristic peaks is 25 cm^{-1}, whereby it can be judged that the MoS$_2$ nanosheet is a 2D structure with few layers or a single layer.[47,48] In addition, the offset difference between the characteristic peaks of the samples does not change after *in situ* growth of AuNPs on the MoS$_2$ nanosheets, indicating that the *in situ* growth of Au does not damage the layered structure of MoS$_2$. The intensity of the two characteristic peaks in Au@MoS$_2$ composite nanosheets is significantly weaker than those of the two characteristic peaks in MoS$_2$ nanosheets, which is the result of the combination of AuNPs and MoS$_2$.

The crystal structure of bulk MoS$_2$, MoS$_2$ nanosheets and Au@MoS$_2$ composite nanosheets were characterized by XRD. As shown in Fig. 2(d), the bulk MoS$_2$ powder corresponds to the standard card (JCPDS no. 00-006-0097), and the main peak of MoS$_2$ nanosheets is located at $2\theta = 14.4°$, which corresponds to

the (002) plane and the standard card (JSPDS no. 77-1716). The main peak at 14.4° is significantly weaker than the diffraction peak of bulk MoS$_2$ crystal powder on the (002) plane, indicating that the MoS$_2$ nanosheets prepared by liquid phase stripping have a regular and few-layer layered stacking structure. In addition, three characteristic peaks of Au@MoS$_2$ composite nanosheets at 38.6°, 44.4° and 64.6°, which corresponds to the (111), (200) and (220) crystal planes of AuNPs,[49] respectively, indicating that AuNPs have been successfully modified on MoS$_2$ nanosheets.

Fig. 3 shows the XPS spectra of MoS$_2$ nanosheets and Au@MoS$_2$ composite nanosheets. All spectral lines were obtained after C 1s calibration with a binding energy of 284.5 eV. It can be seen from Fig. 3 that the main components of the MoS$_2$ nanosheets prepared by us are Mo and S without the interference of other impurities. Moreover, there is no binding energy of MoS$_2$ in the metal phase in the sample. In addition, there is a small peak at 226.7 eV, which can be indexed as S 2 s. The two peaks of Mo 3d$_{5/2}$ and Mo 3d$_{3/2}$ of MoS$_2$ nanosheets are located at 229.5 eV and 232.5 eV,[48] respectively, indicating that the main valence state of Mo element in the nanosheet is +4. The classical peaks of S 2p$_{3/2}$ and S 2p$_{1/2}$ are located at 162.3 eV and 163.5 eV, demonstrating that the main valence state of S element in the nanosheet was −2.

In addition, the high-resolution scanning measurement of Au in Au@MoS$_2$ composite nanosheets revealed that the two peaks of Au 4f$_{5/2}$ and Au 4f$_{7/2}$ in the composite nanosheets are 83.8 eV and 87.5 eV,[50] respectively. The high-intensity Au 4f peaks confirm that Au precursor has been reduced to AuNPs by sodium citrate and has been successfully modified on the surface of MoS$_2$. The XPS spectra of Mo and S of Au@MoS$_2$ composite nanosheets are shown in the ESI Fig. S1.† Compared with the XPS spectra of Mo and S of MoS$_2$ nanosheets, the
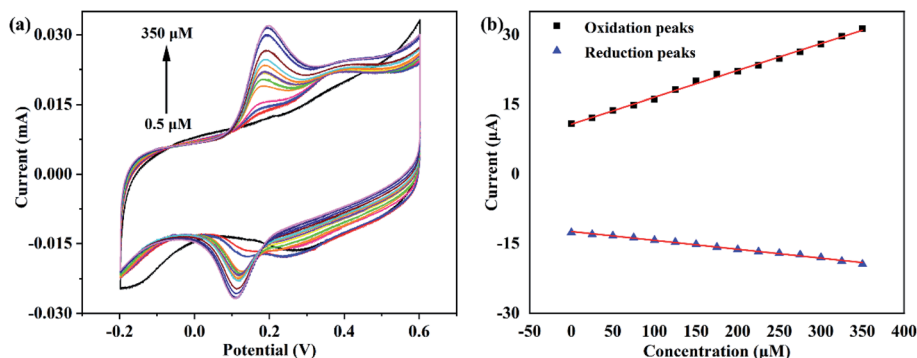

Fig. 6 (a) CV curves of Au@MoS$_2$/GCE in different concentrations of DA; (b) plots of oxidation peaks currents and reduction peaks currents *vs.* concentration of DA.

Table 1 Comparison of the response characteristics of different modified electrodes for detection of DA

Electrode material	Linear range/μM	Detection minimum/μM	References
MWCNT/GONR	0.15–12.15	0.08	51
AuNPs-MoS$_2$	0.05–30	0.05	52
MoS$_2$/RGO	1.5–100	0.94	53
Graphene/PEI/AuNPs	2–48	0.2	54
PEDOT/Pd composite	0.5–1	0.5	55
Graphene	4–100	2.64	56
GNS-CNTs/MoS$_2$	0.1–100	0.05	42
AuNPs@MoS$_2$	0.1–100	0.08	43
Au@MoS$_2$	0.5–350	0.2	This work
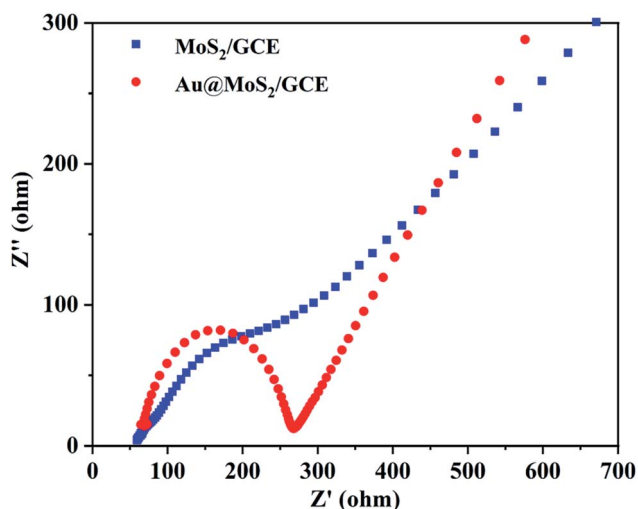
Fig. 7 Nyquist plots of MoS$_2$ GCE and Au@MoS$_2$/GCE.

positions of the binding energy corresponding to each peak does not change.

3.2 Analytical performance of Au@MoS$_2$ modified GCEs

In this work, cyclic voltammetry (CV) was applied to the electrochemical detection of dopamine (DA) using three working electrodes mentioned above as comparators. 150 μM DA was added to 0.1 M PBS solution with pH = 7.0 saturated with N$_2$, and the test was performed in an electrochemical system composed of different electrode materials at a scan rate of 100 mV s^{-1}. The CV curves of DA are shown in Fig. 4. It has been found that the MoS$_2$/GCE exhibits a larger CV area at the same scanning speed compared with the bare GCE. However, neither the bare GCE nor the MoS$_2$/GCE exhibits significant current response or oxidation–reduction peaks after the addition of DA. The CV scanning area of Au@MoS$_2$/GCE under the same scanning conditions greatly exceeds those of the bare GCE and MoS$_2$/GCE. Au nanoparticles significantly increase the response signal. Moreover, it can be clearly observed that the electrode shows a pair of redox peaks corresponding to DA located within the voltage window of 0.1–0.2 V in the electrolyte containing DA besides the oxidation–reduction peaks reflecting its own characteristics. It is indicated that the electrode based on Au@MoS$_2$ composite nanosheets has excellent electrocatalytic

performance towards DA. In addition, in order to prove that Au@MoS$_2$/GCE can stably detect DA, we carried out 50 cycles in PBS buffer containing 150 μM DA, as shown in Fig. S2.† The positions of oxidation–reduction peaks are basically consistent, which proves that electrochemical detection has good stability.

The electrochemical response of DA on Au@MoS$_2$/GCE is attributed to the fact that AuNPs deposited on MoS$_2$ nanosheets provide good electrical conductivity for the material as a whole,[44] increase the active area of the electrodes, and provide pore channels for the conduction of electrons to promote the transmission of electrons, thus improving the current intensity. The electrochemical process of DA is shown in Fig. 5.

To further investigate the analytical performation of the Au@MoS$_2$ modified/GCEs, the effect of different concentrations on the detection of DA by Au@MoS$_2$/GCE at the same scanning speed was also explored, and the linear curves of cyclic voltammetry are shown in Fig. 6(a). From the continuously increasing shape of the CV curves, it can be clearly seen that the current signal increases with the increase of DA concentration, which further illustrates the sensitivity of the Au@MoS$_2$/GCE to DA. Moreover, along with the increase of DA concentration, the oxidation peak current increases and the reduction peak current decreases more obviously.

In order to more accurately reflect the electrocatalytic performance of Au@MoS$_2$/GCE for DA, the data were processed to obtain the relationship between the oxidation peaks current and the reduction peaks current and the concentration of DA as shown in Fig. 6(b). It could be seen that the current values of oxidation peaks and reduction peaks in the CV curves have a good linear relationship with DA concentration. The linear range of DA were 0.5–350 μM. After simulation analysis, the anode regression equation corresponding to oxidation peaks of DA was obtained as $i\,(\mu A) = 10.74917 + 0.05779C\,(\mu M)$, where $R^2 = 0.99717$; the regression equation corresponding to the reduction peaks of DA was $i\,(\mu A) = -12.39725 - 0.01917C\,(\mu M)$, where $R^2 = 0.99422$, indicating that the reliability of the regression equations was worthy of recognition. In addition, the detection limit of the electrode for DA was calculated to be as low as 0.2 μM. Compared with other reported electrochemical biosensors for dopamine detection (Table 1), although the detection limit of the biosensor in this work is not as low as that in ref. 39, 40, 48 and 49, it has the widest detection range
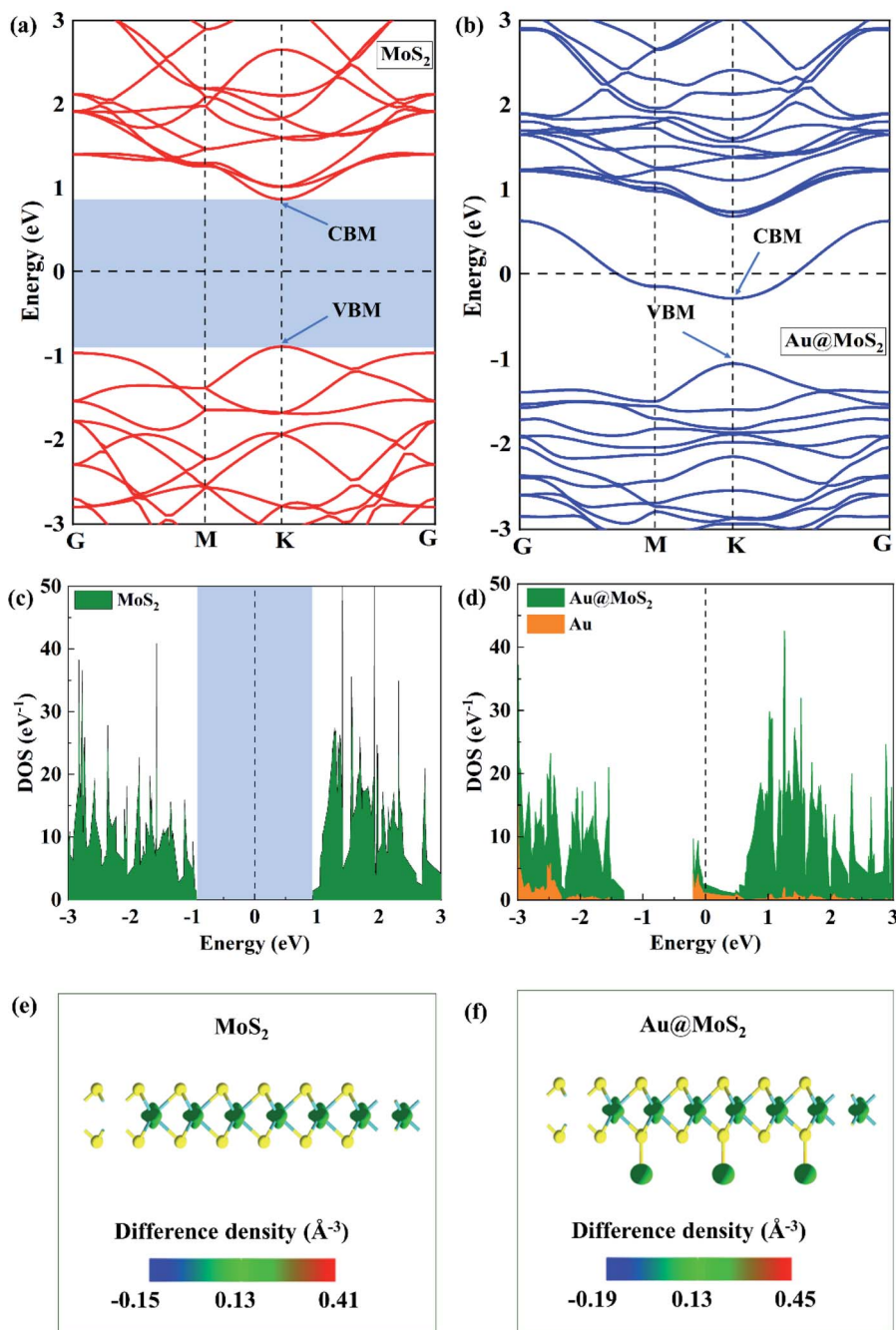
Fig. 8 (a) Band structure of MoS$_2$ nanosheet; (b) band structure of Au@MoS$_2$ composite nanosheet; (c) density of states of MoS$_2$ nanosheet; (d) density of states of Au@MoS$_2$ nanosheet; electronic differential density of (e) MoS$_2$ and (f) Au@MoS$_2$ nanosheets. G, M and K correspond to the (0, 0, 0), (0, 1/2, 0) and (1/3, 1/3, 0) k-points respectively, in the Brillouin zone. The horizontal dashed line marks the Fermi level (the zero of the energy axis in these plots).

compared with all the reference documents in Table 1, and the highest detection range can reach 350 μM. In general, the biosensor of this work yields a relatively wider detection range or a relative lower detection limit. Therefore, we can conclude that the good analytical performance is attributed to the integration of the AuNPs with excellent conductivity and electrocatalytic activity and the MoS$_2$ nanosheets with high surface area.

3.3 Electrochemical behaviors of the MoS$_2$/GCE and Au@MoS$_2$/GCE

Electrochemical impedance spectroscopy (EIS) was an effective method for probing the features of surface modified electrodes, the energy Nyquist diagram of MoS$_2$/GCE and Au@MoS$_2$/GCE was obtained by impedance analysis. Each impedance curve consists of a semicircle in the high frequency region and a linear part in the low frequency region. The slope of the

straight line in the low frequency region represents WuBurg impedance and shows the diffusion rate of ions. The radius of curvature of the semicircular arc represents the reaction resistance R_{ct}, which has a great relationship with the effective contact area of the electrode material and the electrolyte.

As shown in Fig. 7, the slope of the straight part of Au@MoS$_2$/GCE is relatively higher and the radius of curvature is smaller, which indicates that the resistance of electron transfer becomes smaller when AuNPs are modified on the surface of MoS$_2$ nanosheets. Moreover, the result also indicates that Au@MoS$_2$/GCE significantly improved the electrochemical performance of the electrodes.[49]

3.4 Theoretical calculation of MoS$_2$ nanosheets and Au@MoS$_2$ composite nanosheets

In order to in-depth explore the improvement of Au-adsorption on the electrochemical performance of MoS$_2$, the electronic properties of monolayer MoS$_2$ nanosheet before and after Au-adsorption were studied by using the density functional theory (DFT) calculation. For convenience of description, they were expressed as MoS$_2$ and Au@MoS$_2$, respectively. The density of states, electronic differential density as well as the electronic band structure were explored,[57] as shown in Fig. 8. Fig. 8(a) and (b) show the electronic band structures of MoS$_2$ and Au@MoS$_2$. The band gap of MoS$_2$ is calculated to be 1.76 eV, which is consistent with previous research,[58] demonstrating the semiconducting characteristic of the monolayer MoS$_2$ nanosheet.[59] Moreover, its VBM and CBM are both located at K point of hexagonal Brillouin zone, which means that it is a direct band gap semiconductor. But it converts into metallic after adsorbing of Au atoms on the surface of MoS$_2$ nanosheet, because there is a conduct band crosses the Fermi level, indicating that the conductivity of the system is significantly improved. Fig. 8(c) and (d) show the density of states of MoS$_2$ and Au@MoS$_2$ respectively, which is consistent with the above electronic band structure results that the monolayer MoS$_2$ is a semiconductor, because there is an energy gap of 1.76 eV appears at the Fermi level while the Au@MoS$_2$ is a conductor because an obvious DOS peak is observed near the Fermi level. Based on these results, we can conclude that the adsorbed Au atoms play an important role on the contribution of the electrons of the system near the Fermi level. Furthermore, Fig. 8(e) and (f) show the differential electron density diagrams of MoS$_2$ and Au@MoS$_2$, from which we can see that the adsorbed Au atoms contribute to the system electrons to a certain extent.

4. Conclusions

In this work, MoS$_2$ nanosheets were obtained successfully by liquid-phase separation using an ultrasonic crusher, and Au@MoS$_2$ composite nanosheets were successfully prepared in the means of *in situ* growth of AuNPs. Through the characterizations of the XRD diffraction patterns, infrared spectra, ultraviolet-visible spectra, XPS energy spectra, Raman spectra and TEM it was confirmed that the MoS$_2$ nanosheets were in a single layer or a few layers' structure, and the Au@MoS$_2$

composite nanosheets were successfully verified. Furthermore, the electrochemical biosensor with a high-sensitivity for the quantitative electrochemical detection of DA was constructed using the synthesized Au@MoS$_2$ composite nanosheets. The linear detection range was 0.5–350 μm and the detection limit was 0.2 μM, which provides a good foundation for its application in disease diatonics. At the same time, the DFT calculations were the electronic structures of the MoS$_2$ nanosheets and Au@MoS$_2$ composite nanosheets. The results showed that after AuNPs were loaded on the MoS$_2$ nanosheets, the conductivity was significantly improved and the electrochemical performance of the MoS$_2$ nanosheets was improved. This work laid a good foundation for the specific and high sensitivity detection of neurotransmitters.

Conflicts of interest

There are no competing interests to declare.

References

1 M. Samadi, N. Sarikhani, M. Zirak, H. Zhang, H.-L. Zhang and A. Z. Moshfegh, Group 6 transition metal dichalcogenide nanomaterials: synthesis, applications and future perspectives, *Nanoscale Horiz.*, 2018, **3**(2), 90–204.

2 W. Choi, N. Choudhary, G. H. Han, J. Park, D. Akinwande and Y. H. Lee, Recent development of two-dimensional transition metal dichalcogenides and their applications, *Mater. Today*, 2017, **20**(3), 116–130.

3 D. Wang, F. Wu, Y. Song, C. Li and L. Zhou, Large-scale production of defect-free MoS$_2$ nanosheets via pyrene-assisted liquid exfoliation, *J. Alloys Compd.*, 2017, **728**, 1030–1036.

4 Y. Huang, J. Guo, Y. Kang, Y. Ai and C. M. Li, Two dimensional atomically thin MoS$_2$ nanosheets and their sensing applications, *Nanoscale*, 2015, **7**(46), 19358–19376.

5 C. Zhu, Z. Zeng, H. Li, F. Li, C. Fan and H. Zhang, Single-Layer MoS$_2$-Based Nanoprobes for Homogeneous Detection of Biomolecules, *J. Am. Chem. Soc.*, 2013, **135**(16), 5998–6001.

6 A. T. E. Vilian, B. Dinesh, S.-M. Kang, U. M. Krishnan, Y. S. Huh and Y.-K. Han, Recent advances in molybdenum disulfide-based electrode materials for electroanalytical applications, *Microchim. Acta*, 2019, **186**(3), 203.

7 X. Li, J. Shan, W. Zhang, S. Su, L. Yuwen and L. Wang, Recent Advances in Synthesis and Biomedical Applications of Two-Dimensional Transition Metal Dichalcogenide Nanosheets, *Small*, 2017, **13**(5), 1602660.

8 S. Su, H. Sun, W. Cao, J. Chao, H. Peng, X. Zuo, L. Yuwen, C. Fan and L. Wang, Dual-Target Electrochemical Biosensing Based on DNA Structural Switching on Gold Nanoparticle-Decorated MoS$_2$ Nanosheets, *ACS Appl. Mater. Interfaces*, 2016, **8**(11), 6826–6833.

9 S. Su, Y. Wu, D. Zhu, J. Chao, X. Liu, Y. Wan, Y. Su, X. Zuo, C. Fan and L. Wang, On-Electrode Synthesis of Shape-Controlled Hierarchical Flower-Like Gold Nanostructures for Efficient Interfacial DNA Assembly and Sensitive Electrochemical Sensing of MicroRNA, *Small*, 2016, **12**(28), 3794–3801.

10 X. Wang, C. Chu, L. Shen, W. Deng, M. Yan, S. Ge, J. Yu and X. Song, An ultrasensitive electrochemical immunosensor based on the catalytic activity of MoS$_2$-Au composite using Ag nanospheres as labels, *Sens. Actuators, B*, 2015, **206**, 30–36.

11 J. Chao, M. Zou, C. Zhang, H. Sun, D. Pan, H. Pei, S. Su, L. Yuwen, C. Fan and L. Wang, A MoS$_2$-based system for efficient immobilization of hemoglobin and biosensing applications, *Nanotechnology*, 2015, **26**(27), 274005.

12 T. Wang, K. Du, W. Liu, J. Zhang and M. Li, Electrochemical Sensors Based on Molybdenum Disulfide Nanomaterials, *Electroanalysis*, 2015, **27**(9), 2091–2097.

13 N. R. Dalila, M. K. M. Arshad, S. C. B. Gopinath, W. M. W. Norhaimi and M. F. M. Fathil, Current and future envision on developing biosensors aided by 2D molybdenum disulfide (MoS$_2$) productions, *Biosens. Bioelectron.*, 2019, **132**, 248–264.

14 P. Raj, M. H. Oh, K. Han and T. Y. Lee, Label-Free Electrochemical Biosensor Based on Au@MoS$_2$-PANI for Escherichia coli Detection, *Chemosensors*, 2021, **9**(3), 49.

15 Y. Ou, A. M. Buchanan, C. E. Witt and P. Hashemi, Frontiers in electrochemical sensors for neurotransmitter detection: towards measuring neurotransmitters as chemical diagnostics for brain disorders, *Anal. Methods*, 2019, **11**(21), 2738–2755.

16 M. O. Klein, D. S. Battagello, A. R. Cardoso, D. N. Hauser, J. C. Bittencourt and R. G. Correa, Dopamine: Functions, Signaling, and Association with Neurological Diseases, *Cell. Mol. Neurobiol.*, 2019, **39**(1), 31–59.

17 S. D. Niyonambaza, A. Koudrina, M. C. DeRosa, M. Boukadoum, A. Miled and E. Boisselier, Aptamer-Modified Ultrastable Gold Nanoparticles for Dopamine Detection, *IEEE Sens. J.*, 2021, **21**(3), 2517–2525.

18 Y. Li, H. Lin, H. Peng, R. Qi and C. Luo, A glassy carbon electrode modified with MoS$_2$ nanosheets and poly(3,4-ethylenedioxythiophene) for simultaneous electrochemical detection of ascorbic acid, dopamine and uric acid, *Microchim. Acta*, 2016, **183**(9), 2517–2523.

19 B. Si and E. Song, Recent Advances in the Detection of Neurotransmitters, *Chemosensors*, 2018, **6**(1), 1.

20 Z. Shi, X. Wu, Z. Zou, L. Yu, F. Hu, Y. Li, C. Guo and C. M. Li, Screen-printed analytical strip constructed with bacteria-templated porous N-doped carbon nanorods/Au nanoparticles for sensitive electrochemical detection of dopamine molecules, *Biosens. Bioelectron.*, 2021, 186.

21 S. S. Choo, E. S. Kang, I. Song, D. Lee, J. W. Choi and T. H. Kim, Electrochemical Detection of Dopamine Using 3D Porous Graphene Oxide/Gold Nanoparticle Composites, *Sensors*, 2017, **17**(4), 861.

22 I. R. Suhito, N. Angeline and T.-H. Kim, Nanomaterial-modified Hybrid Platforms for Precise Electrochemical Detection of Dopamine, *BioChip J.*, 2019, **13**(1), 20–29.

23 S. Hannah, M. Al-Hatmi, L. Gray and D. K. Corrigan, Low-cost, thin-film, mass-manufacturable carbon electrodes for detection of the neurotransmitter dopamine, *Bioelectrochemistry*, 2020, **133**, 107480.

24 D.-S. Kim, E.-S. Kang, S. Baek, S.-S. Choo, Y.-H. Chung, D. Lee, J. Min and T.-H. Kim, Electrochemical detection of dopamine using periodic cylindrical gold nanoelectrode arrays, *Sci. Rep.*, 2018, **8**(1), 14049.

25 H. Du, X. Zhang, Z. Liu and F. Qu, A supersensitive biosensor based on MoS$_2$ nanosheet arrays for the real-time detection of H$_2$O$_2$ secreted from living cells, *Chem. Commun.*, 2019, **55**(65), 9653–9656.

26 S. Su, M. Zou, H. Zhao, C. Yuan, Y. Xu, C. Zhang, L. Wang, C. Fan and L. Wang, Shape-controlled gold nanoparticles supported on MoS$_2$ nanosheets: synergistic effect of thionine and MoS$_2$ and their application for electrochemical label-free immunosensing, *Nanoscale*, 2015, **7**(45), 19129–19135.

27 S. P. Selvam, M. Hansa and K. Yun, Simultaneous differential pulse voltammetric detection of uric acid and melatonin based on a self-assembled Au nanoparticle-MoS$_2$ nanoflake sensing platform, *Sens. Actuators, B*, 2020, **307**, 127683.

28 Y. L. Hu, Y. Huang, C. L. Tan, X. Zhang, Q. P. Lu, M. Sindoro, X. Huang, W. Huang, L. H. Wang and H. Zhang, Two-dimensional transition metal dichalcogenide nanomaterials for biosensing applications, *Mater. Chem. Front.*, 2017, **1**(1), 24–36.

29 Y. Ling, T. T. Cao, L. B. Liu, J. L. Xu, J. Zheng, J. X. Li and M. Zhang, Fabrication of noble metal nanoparticles decorated on one dimensional hierarchical polypyrrole@MoS$_2$ microtubes, *J. Mater. Chem. A*, 2020, **8**(34), 7801–7811.

30 J. Zheng, D. D. Song, H. Chen, J. L. Xu, N. S. Alharbi, T. Hayat and M. Zhang, Enhanced peroxidase-like activity of hierarchical MoS$_2$-decorated N-doped carbon nanotubes with synergetic effect for colorimetric detection of H$_2$O$_2$ and ascorbic acid, *Chin. Chem. Lett.*, 2020, **31**(5), 1109–1113.

31 F. Wang, C. L. Chi, B. Yu and B. Ye, Simultaneous voltammetric determination of dopamine and uric acid based on Langmuir-Blodgett film of calixarene modified glassy carbon electrode, *Sens. Actuators, B*, 2015, **221**, 1586–1593.

32 C. Wang, J. Du, H. Wang, C. e. Zou, F. Jiang, P. Yang and Y. Du, A facile electrochemical sensor based on reduced graphene oxide and Au nanoplates modified glassy carbon electrode for simultaneous detection of ascorbic acid, dopamine and uric acid, *Sens. Actuators, B*, 2014, **204**, 302–309.

33 H. R. Rees, S. E. Anderson, E. Privman, H. H. Bau and B. J. Venton, Carbon Nanopipette Electrodes for Dopamine Detection in Drosophila, *Anal. Chem.*, 2015, **87**(7), 3849–3855.

34 A. G. Zestos, C. Yang, C. B. Jacobs, D. Hensley and B. J. Venton, Carbon nanospikes grown on metal wires as microelectrode sensors for dopamine, *Analyst*, 2015, **140**(21), 7283–7292.

35 L. Tang, D. Du, F. Yang, Z. Liang, Y. Ning, H. Wang and G.-J. Zhang, Preparation of Graphene-Modified Acupuncture Needle and Its Application in Detecting Neurotransmitters, *Sci. Rep.*, 2015, **5**(1), 11627.

36 S.-S. Choo, E.-S. Kang, I. Song, D. Lee, J.-W. Choi and T.-H. Kim, Electrochemical Detection of Dopamine Using 3D Porous Graphene Oxide/Gold Nanoparticle Composites, *Sensors*, 2017, **17**(4), 861.

37 Y. Ling and Y. Xia, Gold Based Nanocomposites: Fabrication Strategies, Properties, and Tumor Theranostic Applications, *Acta Physica-Chimica Sinica*, 2020, **36**(9), 88–102.

38 S. Su, W. Cao, C. Zhang, X. Han, H. Yu, D. Zhu, J. Chao, C. Fan and L. Wang, Improving performance of MoS_2-based electrochemical sensors by decorating noble metallic nanoparticles on the surface of MoS_2 nanosheet, *RSC Adv.*, 2016, **6**(80), 76614–76620.

39 L. Guardia, J. I. Paredes, R. Rozada, S. Villar-Rodil, A. Martinez-Alonso and J. M. D. Tascon, Production of aqueous dispersions of inorganic graphene analogues by exfoliation and stabilization with non-ionic surfactants, *RSC Adv.*, 2014, **4**(27), 14115–14127.

40 J. Lu, M. Chen, L. Dong, L. Cai, M. Zhao, Q. Wang and J. Li, Molybdenum disulfide nanosheets: From exfoliation preparation to biosensing and cancer therapy applications, *Colloids Surf. B Biointerfaces*, 2020, 194.

41 Y. Liu and R. Li, Study on ultrasound-assisted liquid-phase exfoliation for preparing graphene-like molybdenum disulfide nanosheets, *Ultrason. Sonochem.*, 2020, 63.

42 V. Mani, M. Govindasamy, S.-M. Chen, R. Karthik and S.-T. Huang, Determination of dopamine using a glassy carbon electrode modified with a graphene and carbon nanotube hybrid decorated with molybdenum disulfide flowers, *Microchim. Acta*, 2016, **183**(7), 2267–2275.

43 S. Su, H. Sun, F. Xu, L. Yuwen and L. Wang, Highly Sensitive and Selective Determination of Dopamine in the Presence of Ascorbic Acid Using Gold Nanoparticles-Decorated MoS_2 Nanosheets Modified Electrode, *Electroanalysis*, 2013, **25**(11), 2523–2529.

44 K.-J. Huang, Y.-J. Liu, Y.-M. Liu and L.-L. Wang, Molybdenum disulfide nanoflower-chitosan-Au nanoparticles composites based electrochemical sensing platform for bisphenol A determination, *J. Hazard. Mater.*, 2014, **276**, 207–215.

45 S. Su, W. Cao, W. Liu, Z. Lu, D. Zhu, J. Chao, L. Weng, L. Wang, C. Fan and L. Wang, Dual-mode electrochemical analysis of microRNA-21 using gold nanoparticle-decorated MoS_2 nanosheet, *Biosens. Bioelectron.*, 2017, **94**, 552–559.

46 K. Shomalian, M. M. Bagheri-Mohagheghi and M. Ardyanian, Characterization and study of reduction and

sulfurization processing in phase transition from molybdenum oxide (MoO_2) to molybdenum disulfide (MoS_2) chalcogenide semiconductor nanoparticles prepared by one-stage chemical reduction method, *Appl. Phys. A: Mater. Sci. Process.*, 2017, **123**(1), 1–9.

47 C. Liu, F. Jia, Q. Wang, B. Yang and S. Song, Two-dimensional molybdenum disulfide as adsorbent for high-efficient Pb(II) removal from water, *Appl. Mater. Today*, 2017, **9**, 220–228.

48 Y. Yan, B. Xia, X. Ge, Z. Liu, J.-Y. Wang and X. Wang, Ultrathin MoS_2 Nanoplates with Rich Active Sites as Highly Efficient Catalyst for Hydrogen Evolution, *ACS Appl. Mater. Interfaces*, 2013, **5**(24), 12794–12798.

49 Y. Zhai, J. Li, X. Chu, M. Xu, F. Jin, X. Fang, Z. Wei and X. Wang; IEEE, Preparation of Au-MoS_2 Electrochemical Electrode and Investigation on Glucose Detection Characteristics. in *2016 6th IEEE International Conference on Manipulation, Manufacturing and Measurement on the Nanoscale*, 2016, pp. 287–290.

50 Y. Yuan, B. Yang, F. Jia and S. Song, Reduction mechanism of Au metal ions into Au nanoparticles on molybdenum disulfide, *Nanoscale*, 2019, **11**(19), 9488–9497.

51 C.-L. Sun, C.-T. Chang, H.-H. Lee, J. Zhou, J. Wang, T.-K. Sham and W.-F. Pong, Microwave-Assisted Synthesis of a Core-Shell MWCNT/GONR Heterostructure for the Electrochemical Detection of Ascorbic Acid, Dopamine, and Uric Acid, *ACS Nano*, 2011, **5**(10), 7788–7795.

52 H. Sun, J. Chao, X. Zuo, S. Su, X. Liu, L. Yuwen, C. Fan and L. Wang, Gold nanoparticle-decorated MoS_2 nanosheets for simultaneous detection of ascorbic acid, dopamine and uric acid, *RSC Adv.*, 2014, **4**(52), 27625–27629.

53 K. Pramoda, K. Moses, U. Maitra and C. N. R. Rao, Superior Performance of a MoS_2-RGO Composite and a Borocarbonitride in the Electrochemical Detection of Dopamine, Uric Acid and Adenine, *Electroanalysis*, 2015, **27**(8), 1892–1898.

54 V. K. Ponnusamy, V. Mani, S.-M. Chen, W.-T. Huang and J.-F. Jen, Rapid microwave assisted synthesis of graphene nanosheets/polyethyleneimine/gold nanoparticle composite and its application to the selective electrochemical determination of dopamine, *Talanta*, 2014, **120**, 148–157.

55 S. Harish, J. Mathiyarasu, K. L. N. Phani and V. Yegnaraman, PEDOT/Palladium composite material: synthesis, characterization and application to simultaneous determination of dopamine and uric acid, *J. Appl. Electrochem.*, 2008, **38**(11), 1583–1588.

56 Y.-R. Kim, S. Bong, Y.-J. Kang, Y. Yang, R. K. Mahajan, J. S. Kim and H. Kim, Electrochemical detection of dopamine in the presence of ascorbic acid using graphene modified electrodes, *Biosens. Bioelectron.*, 2010, **25**(10), 2366–2369.

57 Y. Xie and Y. Wang, Electronic structure and electrochemical performance of CoS_2/MoS_2 nanosheet composite: Simulation calculation and experimental investigation, *Electrochim. Acta*, 2020, 364.

58 A. Splendiani, L. Sun, Y. Zhang, T. Li, J. Kim, C.-Y. Chim, G. Galli and F. Wang, Emerging Photoluminescence in Monolayer MoS$_2$, *Nano Lett.*, 2010, **10**(4), 1271–1275.

59 Y. Xie, Synthesis and Bandgap Tuning of Novel Germanium and Silicon based Semiconductor Two-Dimensional Atomic Crystals, *Acta Physica-Chimica Sinica*, 2020, **36**(11), 25–26.